

## Article

# Enhanced Multimodal Effect of Chemotherapy, Hyperthermia and Magneto-Mechanic Actuation of Silver-Coated Magnetite on Cancer Cells

Dumitru Daniel Herea <sup>1</sup>, Camelia-Mihaela Zară-Dănceanu <sup>1,\*</sup>, Luminița Lăbușcă <sup>1,2,\*</sup>, Anca-Emanuela Minuti <sup>1,3</sup>, Cristina Stăvilă <sup>1,3</sup>, Gabriel Ababei <sup>1</sup>, Mihai Tibu <sup>1</sup>, Marian Grigoraș <sup>1</sup>, Mihaela Lostun <sup>1</sup>, George Stoian <sup>1</sup>, Oana-Georgiana Dragoș-Pînzaru <sup>1</sup>, Gabriela Buema <sup>1</sup>, Horia Chiriac <sup>1</sup> and Nicoleta Lupu <sup>1</sup>

<sup>1</sup> Department of Magnetic Materials and Devices, National Institute of Research and Development for Technical Physics, 700050 Iasi, Romania

<sup>2</sup> Orthopedics and Traumatology Clinic, County Emergency Hospital Saint Spiridon Iasi, 700111 Iasi, Romania

<sup>3</sup> Faculty of Physics, Alexandru Ioan Cuza University, 700506 Iasi, Romania

\* Correspondence: cdanceanu@phys-iasi.ro (C.-M.Z.-D.); llabusca@phys-iasi.ro (L.L.)

**Abstract:** Currently, various methods based on magnetic nanoparticles are being considered for the treatment of cancer. Among these, magnetic hyperthermia and magneto-mechanical actuation are the most tested physical methods that have shown promising results when applied both separately and in combination. However, combining them with specific drugs can further improve antitumor efficiency. In this study, we performed a systematic analysis to determine the best combination of hyperthermia, magneto-mechanical actuation of silver-coated magnetite nanoparticles (MNP@Ag) and chemotherapy (mitoxantrone) capable of destroying tumor cells *in vitro* while maintaining normal cells in their state of increased viability. The results showed that of the nine treatment configurations, the only one that satisfied the safety condition for normal cells (fibroblasts) and the highly cytotoxic condition for tumor cells (HeLa) was the combination of all three triggers. This combination led to the decrease in HeLa viability to about 32%, while the decrease in fibroblast viability reached 80%. It was observed that the cytotoxic effect was not a sum of the separate effects of each trigger involved, but the result of a nonlinear conjugation of the triggers in a dynamic regime imposed by the magneto-mechanical actuation of the nanoparticles. We conclude that by using such a treatment approach, the need for chemotherapeutic drugs can be substantially reduced while maintaining their therapeutic performance.

**Keywords:** silver-coated nanoparticles; hyperthermia; magneto-mechanic actuation; mitoxantrone; tumor cells



**Citation:** Herea, D.D.; Zară-Dănceanu, C.-M.; Lăbușcă, L.; Minuti, A.-E.; Stăvilă, C.; Ababei, G.; Tibu, M.; Grigoraș, M.; Lostun, M.; Stoian, G.; et al. Enhanced Multimodal Effect of Chemotherapy, Hyperthermia and Magneto-Mechanic Actuation of Silver-Coated Magnetite on Cancer Cells. *Coatings* **2023**, *13*, 406. <https://doi.org/10.3390/coatings13020406>

Academic Editor: Gianni Barucca

Received: 16 January 2023

Revised: 3 February 2023

Accepted: 7 February 2023

Published: 10 February 2023



**Copyright:** © 2023 by the authors. Licensee MDPI, Basel, Switzerland. This article is an open access article distributed under the terms and conditions of the Creative Commons Attribution (CC BY) license (<https://creativecommons.org/licenses/by/4.0/>).

## 1. Introduction

Nanotechnology has imposed itself as a potent tool in a large variety of life science and medical applications. Nanomedicine, the application of nanotechnology in the medical field, is already enlarging the clinical field of diagnostic tools, drug delivery and medical sensors [1]. One particular field of development for nanomedical systems is cancer therapy [2]. Despite decades of research for the development of advanced therapies, cancer diagnostic and treatment remain an unsolved problem [3]. Even though cancer mortality has declined over the last three decades in high-income countries, there are persisting and substantial differences in mortality, incidence, and survival worldwide with more than 19.3 million new cases and almost 10.0 million cancer deaths occurring as per 2020 [4]. One of the most efficient approaches in treating malignancies is to combine different therapeutic principles. The so-called multimodal therapeutic approach has been recognized as a modality to increase efficiency, avoid side effects as well as the cancer relapse associated with

cell heterogeneity within a tumor and/or metastatic dissemination [5]. Multimodal cancer therapy has benefited from noble metals such as gold nanoparticles which have shown a fine potential in backing the chemotherapy and radiotherapy treatments [6]. Magnetic nanoparticles (MNPs) are intensely scrutinized for their potential to serve as drug carriers and theranostic agents [7]. Tumor theranostics represent the combination of diagnosis and therapy to cure cancer, aiming to reduce delays in treatment and thus to improve patient care [8]. Due to their high versatility to be straightforwardly produced with tuned sizes, shapes and magnetic properties, MNPs have shown a significant role in improving a series of conventional or new biomedical methods and techniques. Ranging generally from clusters of several atoms to structures up to 100 nm—at least in one dimension—the MNPs are endowed with peculiar characteristics such as an enlarged surface-to-volume ratio, enhanced surface spin disorder, and various regular and irregular shapes, which allow, through subsequent surface-related modifications, the development of new core-shell magnetic materials for cutting-edge biomedical applications. MNPs, with their distinct class of iron oxides, were coated with amphiphilic polymers [9] polysaccharides [10], graphene [11], silica [12], gold [13], silver [14–19], etc. The latter displayed unique physical and chemical properties including optical, electrical, and thermal ones [20]. Consequently, silver nanoparticles are being intensively explored for various applications due to their specific physicochemical characteristics such as large surface-area-to-volume ratio, increased surface plasmon resonance, and ease of ligand functionalization [21]. Accordingly, they were tested for different biomedical applications due to their antibacterial, antiviral, antifungal, anti-inflammatory, anti-angiogenic, and antitumor effects [20,22]. Silver and silver nanoparticles have been recently shown to exert cytotoxic effects on cancer cells but not on normal cells, being proposed as a tumor theranostic agent [23].

By endowing silver nanoparticles with magnetic properties, their spectrum of biomedical applications is rapidly expanded to magnetic hyperthermia, magnetic drug delivery, magneto-mechanical actuation, magnetic separation, MRI imaging, and so on, virtually covering the entire spectrum of applications attributed to magnetic nanoparticles. Thus, these hybrid nanoparticles simultaneously provide all the specific magnetic benefits of the magnetic core together with all the advantages of the silver shell described above.

The remote magnetic actuation of MNPs incubated with tumor cells can trigger a mechanical hit and vibrations on tumor cells, leading to their irreversible damage. Basically, the alternating magnetic fields constantly change the position of the MNPs depending on the field gradients and frequency, to generate torques onto the cells [24]. Such torques can modify the level of calcium entry within cells, stimulate drug release, induce protein degradation, generate high-stemness tumor cells from different cancer cell lines, or destroy cancer cells [24,25].

We have previously reported on the efficiency of magnetically actuated MNPs in destroying cancer cells [26], on the ability of MNP loaded with an antitumoral agent (mitoxantrone) to target tumor-like tissue *in vitro* [27], and on the use of new alloy particles for self-controlled magnetic hyperthermia [28,29]. In this work, we sought to investigate systematically the *in vitro* action of a conventional antitumor drug, non-magnetic hyperthermia, and the magneto-mechanical actuation of silver-coated MNPs (MNP@Ag), applied separately or in combination, on HeLa-cell survival. Our previous experiments [30] have shown that the uncoated magnetite cannot be used to treat tumor cells simply because cancer cells grow and proliferate exceptionally well in the presence of an iron source. The final goal of the work was to find the best combination for the most efficient therapeutic effect seeking to decrease the antitumor drug dose to obtain similar tumor cell damage as in the case of a full dose.

## 2. Materials and Methods

All reagents used for the silver-coated MNP, i.e., ferrous chloride tetrahydrate, ( $\text{FeCl}_2 \cdot 4\text{H}_2\text{O}$ ; 98%), ferric chloride hexahydrate, ( $\text{FeCl}_3 \cdot 6\text{H}_2\text{O}$ ; 98%), sodium hydroxide (NaOH; 98%), mitoxantrone, fibroblast cells and HeLa tumor cells were purchased from

Sigma-Aldrich (Darmstadt, Germany) and used without any further purification. Silver nitrate was purchased from Alfa Aesar—Thermo Fisher (Kandel, Germany). For characterization, the particles were used either as powders or colloids. For dry state characterization, the magnetic nanoparticles were kept at 90 °C for 3 h. For colloid evaluation, the suspensions were sonicated in pulses.

### 2.1. Synthesis of Magnetic Nanoparticles

A measure of 1.1 g  $\text{FeCl}_2 \cdot 4\text{H}_2\text{O}$  was dissolved in 10 mL of ultrapure water and filtered through a 220 nm filter. Then, 3 g of  $\text{FeCl}_3 \cdot 6\text{H}_2\text{O}$  was mixed with the freshly prepared  $\text{FeCl}_2$  solution and the resulting solution was filtered through a 220 nm filter. Next, 2 mL of ultrapure water was used to wash the filter and added to the iron solution. The solution was added over 400 mL of heated ultrapure water (about 90 °C), under magnetic stirring (800 rpm—MS7-H550-Pro, Onilab, City of Industry, CA, USA), followed by careful addition of solid NaOH (15 g). The solution immediately turned black. After 2 min, the heating was stopped, while the stirring continued for 60 min. Then, the suspension was sonicated for 1 h in an ultrasound bath. The magnetic nanoparticles were washed several times with ultrapure water until the pH was about 6. Afterwards, the obtained suspension (about 80 mL) was ultrasonicated for 40 min through an ultrasonic homogenizer with probe, at 100% amplitude.

### 2.2. Synthesis of Silver-Coated Magnetic Nanoparticles (MNP@Ag)

A measure of 40 mL of MNP suspension (14.5 mg/mL MNP) was mixed with 25 mL trisodium citrate (concentration 10 mg/mL, (Thermo Fisher, Kandel, Germany), ultrasonicated for 5 min, and added over 400 mL of heated ultrapure water (about 95 °C), under magnetic stirring (1000 rpm). After 0.5–1 min, 25 mL of filtered  $\text{AgNO}_3$  (200 mg) (Thermo Fisher, Kandel, Germany) were quickly added to the MNP-citrate suspension. Then, the suspension was stirred for 2 h at 800 rpm and about 95 °C.

### 2.3. Cell Viability Evaluation

For cytotoxicity assays, the utilized suspensions of silver-coated MNPs were first submitted to autoclavation (121 °C, 1.5 bar). Dermal fibroblast cells and tumor cells, respectively, were plated in 96 well plates, at  $2 \times 10^4$  cells/well and incubated for 48 h. Each well was filled with 190  $\mu\text{L}$  complete cell culture media (CCM), i.e., Dulbecco Modified Essential Medium DMEM (Sigma Life Science, St. Louis, MO, USA) supplemented with 10% fetal bovine serum (FBS, Sigma Life Science, St. Louis, MO, USA) and 1% antibiotic-antimycotic (Sigma Aldrich, St. Louis, MO, USA). Then, 10  $\mu\text{L}$  of silver-coated MNPs (concentration about 0.3 mg/mL) was added to each well, each sample in triplicate and further incubated for 24 h. Cell viability tests were performed using 5-Dimethylthiazol-2-yl-2, 5-diphenyltetrazolium bromide (MTT, Sigma Life Science, St. Louis, MO, USA) assay (Vybrant MTT cell proliferation assay Sigma Life Science, St. Louis, MO, USA) accordingly to supplier's instructions; dimethylsulfoxide (DMSO, Sigma Aldrich, St. Louis, MO, USA) was used as dilution agent. Absorbance was read at 570 nm. Cell viability (CV) as expressed by optical density (OD) was calculated using the formula  $\text{CV} = 100 \times (\text{ODs} - \text{ODb}) / (\text{ODc} - \text{ODb})$ , where ODs = OD of particle treated cells; ODb = OD of blank (media only); ODc = OD of untreated cells. For particle-free viability evaluation, the protocol was identical, except that the wells were filled with 200  $\mu\text{L}$  CCM.

### 2.4. Magneto-Mechanic Actuation of MNP@Ag

For magnetic field generation, a conventional Helmholtz system consisting of two coils was used. The proprietary software that controlled the coils allowed us to set the magnetic field intensity, its frequency and exposure time. The coil system was fed by waveforms generated using a code realized in LabView. The culture plates were placed in the center of the coil system, where the magnetic field is uniform. The intensity of the magnetic field was 12 G, and was shifted by 180° with a frequency of 2 Hz. The system can generate fields

from 1 to 40 Oe. The coil was introduced inside a CO<sub>2</sub> cell culture incubator (Figure 1). The MMA was applied for 1h, five times, over three days (twice a day).

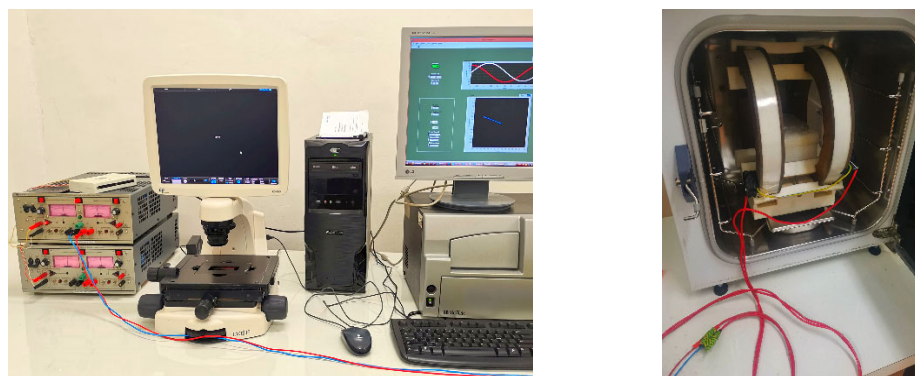


**Figure 1.** Experimental setup. Left—PC with the proprietary software to control the current passing through the coils; National Instruments acquisition board; and Kepco-Bop bipolar power amplifier. Right—the Helmholtz coil system inside the CO<sub>2</sub> cell culture incubator.

### 2.5. Hyperthermia Generation

In order to increase the temperature of the cells, we used a cell culture incubator. Compared to magnetic hyperthermia, this setup comes with several advantages: (a) the sterile conditions are continuously preserved for cell culture; (b) the temperature is well controlled and rigorously kept fixed throughout cell culture; (c) the 5% CO<sub>2</sub> atmosphere is continuously provided; (d) the humidity conditions are not affected. Practically, the conditions were kept similar for the control cells which were placed in another cell incubator at 37 °C. Therefore, the reliability of this approach affords the guarantee of a fine reproducibility of the experiments. The HT was applied for 1 h, five times, over three days (twice a day).

### 2.6. Characterization Equipment

X-ray diffraction patterns were recorded using a Bruker AXS D8-Advance powder X-ray diffractometer (CuK $\alpha$  radiation,  $\lambda = 0.1541$  nm, Bruker, Karlsruhe, Germany). Electron micrographs of the powders were taken by using a FIB/FE-SEM CrossBeam Carl Zeiss NEON 40 EsB equipped (Carl Zeiss SMT GmbH, Oberkochen, Germany) with an energy dispersive X-ray spectroscopy (EDS, Carl Zeiss SMT GmbH, Oberkochen, Germany) module for compositional studies. The magnetization data were acquired on a Lake Shore 7410 vibrating sample magnetometer (VSM, Lake Shore Cryotronics, Westerville, OH, USA). The morphology of the nanoparticles was determined through an ultra-high resolution transmission electron microscopy (UHR-TEM) (Libra 200 UHR-TEM, Carl Zeiss, Oberkochen, Germany). Mean sizes and size distribution of the as-prepared aqueous suspension of nanoparticles were evaluated through a dynamic light scattering (DLS) technique using a scattering spectrometer (Nanotracer NPA 252, Microtrac, Montgomeryville, PA, USA). UV-VIS absorption spectra were recorded with Synergy HTX multimode reader (BioTek Instruments, Santa Clara, CA, USA). Zeta potential was measured using a particle size analyzer (Beckman Coulter, Brea, CA, USA). Ultrasonication of the samples was performed with an ultrasound bath, and an ultrasonic homogenizer (UP50H, Hielscher Ultrasonics GmbH, Teltow, Germany), at 90% amplitude, respectively. The measurements and in vitro testing were performed from the stable, unsettled suspensions of nanoparticles.

Statistical analysis. All the experiments were performed in triplicate. Statistical analysis was performed using Microsoft Excel 2013 to calculate the mean  $\pm$  SD (standard deviation), and Origin 2019 and Microsoft Excel 2013 to test for differences between means through analysis of variance (ANOVA) analysis with a post hoc Tukey's test, and Student *t*-test, respectively.

### 3. Results and Discussions

**XRD analysis.** The XRD patterns of the MNPs and MNP@Ag (Figure 2) showed specific diffraction peaks of magnetite at  $30.2^\circ$ ,  $35.5^\circ$ ,  $43.2^\circ$ ,  $53.6^\circ$ ,  $57.2^\circ$  and  $62.9^\circ$ , corresponding to (220), (311), (400), (422), (511) and (440) crystalline planes of magnetite phase, respectively [31], along with diffraction peaks of silver at  $38.3^\circ$ ,  $44.3^\circ$ ,  $64.5^\circ$ , corresponding to (111), (200) and (220) diffraction planes. The Bragg reflections pointed out a face-centered cubic structure of metallic silver.

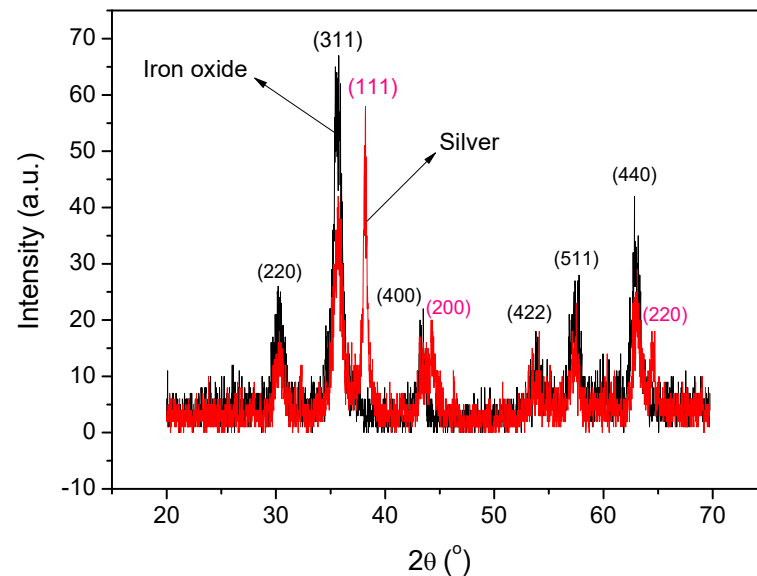


**Figure 2.** XRD patterns of iron oxide (MNP: black line) and MNP@Ag (red line).

**UV–VIS spectroscopy.** The spectra of MNP MNP@Ag solutions were recorded from 300 to 700 nm. Figure 3 shows an absorption peak at 402 nm for MNP@Ag. However, after subtracting the UV–VIS spectra of the MNP from MNP@Ag to obtain only the contribution of the silver shell, the absorption peak shifted to 412 nm. The obtained peaks were in the specific surface plasmon resonance range (400–500 nm) described for silver nanoparticles [31,32], demonstrating the presence of silver in the magnetic suspension. HRTEM mapping (Figure 4) also confirmed the presence of silver in the samples.

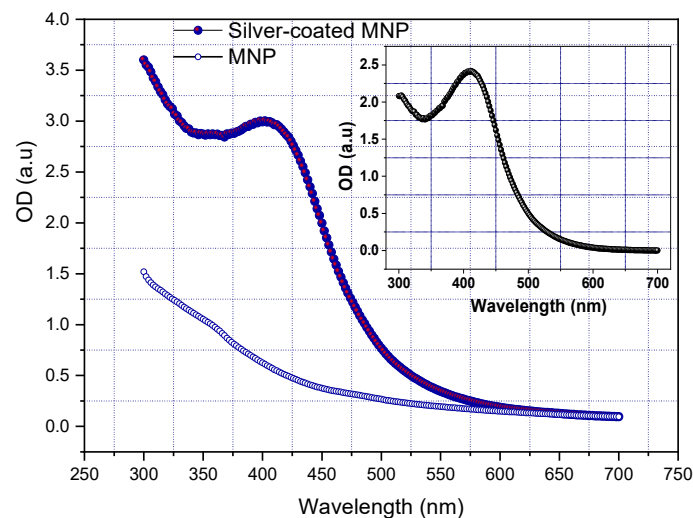


**Figure 3.** UV–Vis spectra of MNP and MNP@Ag, respectively. Inset: UV–Vis spectrum resulting from subtracting the UV–Vis spectra of the MNP from MNP@Ag.

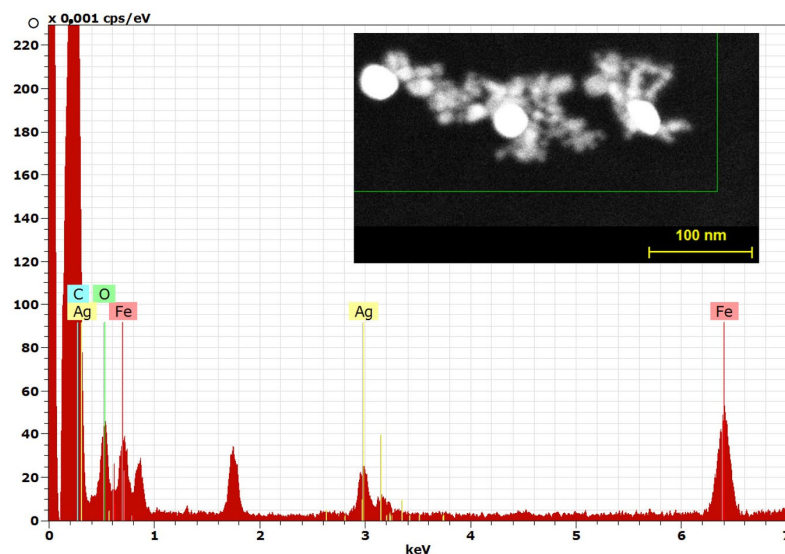


Figure 4. HRTEM element mapping of the silver-coated magnetite.

DLS analysis also used non-filtered (as-prepared) solutions of the nanoparticles, after short sonication. The obtained data showed a narrow size distribution for both samples with mean sizes of 39.2 nm for MNP and 40.5 nm for MNP@Ag (Figure 5). However, the mean sizes provided by the DLS method took into account the hydrodynamic diameter of the particles and, therefore, they seemed to be bigger. The size distribution data of MNP@Ag sample pointed out a low fraction (0.11%) of nanoparticles of about 102 nm—confirmed by TEM measurements—that were not present in the MNP sample. Most probably, this fraction contributed the most to the settlement formation. Otherwise, except for the tiny settlement, the suspension turned out to be very stable for several months.

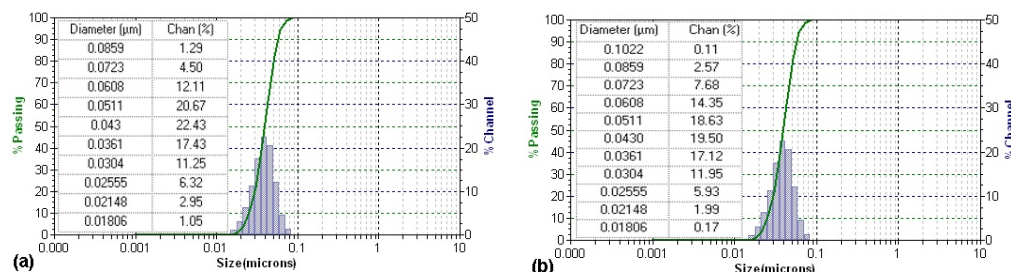
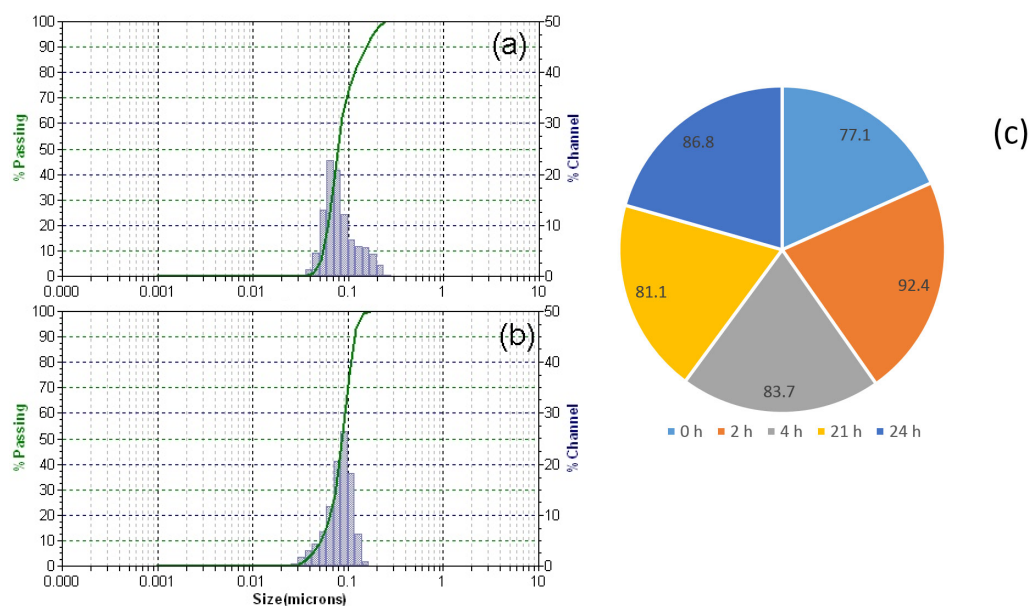


Figure 5. DLS histograms showing the size distribution of (a) MNP and (b) MNP@Ag.

The zeta potential of the MNP@Ag was found to be  $-40.26$  mV, also indicating excellent stability in aqueous solutions. The strong electrostatic repulsion most probably overcame the low magnetic attraction between the nanoparticles. The stability extended to several months and was also empirically observed for the aqueous suspensions of MNP@Ag nanoparticles.

However, since it was not clear how stable the MNP@Ag nanoparticles were after incubation cells, we performed DLS measurements of MNP@Ag dispersed in cell culture medium. The size distribution of MNP@Ag was measured at different time intervals, including one after 24 h, without disturbing the suspension. The results showed that, after mixing with the culture medium, the hydrodynamic diameter of the particles increased from about 40 nm (measured in ultrapure water) to 80–90 nm (Figure 6).



**Figure 6.** DLS histograms showing the size distribution of MNP@Ag nanoparticles immediately after mixing with cell culture medium (a), and after 24 h (b). The mean hydrodynamic diameters of the MNP@Ag nanoparticles at different times (c).

No sediment was observed in the cuvette of the Nanotracs/Microtracs sizer, containing the suspension, after 24 h. Therefore, the suspension was stable over 24 h in the cell culture medium, but the hydrodynamic diameter doubled. This can be attributed first to the formation of the protein corona on the surface of the nanoparticles. Second, clusters of several nanoparticles could not be excluded. However, the suspension remained stable over 24 h, while the size distribution remained almost unchanged for this period.

**TEM and SEM analysis.** Electron microscopy measurements showed magnetite nanoparticles with different prismatic shapes, and sizes below 30 nm (Figure 7a,b). Silver-coated magnetite nanoparticles displayed similar geometries as magnetite nanoparticles, with sizes slightly higher (Figure 7c,f). However, there was also observed a spot of bigger silver-coated nanoparticles (about 30–80 nm in diameter) with round shapes (Figure 7d). This fraction of nanoparticles was also detected and measured by the DLS technique (Figure 5). It was visible in a separate spot most probably because the provided aliquot sample for TEM measurements remained undisturbed for several days until carefully taken and dispersed on the grids. This time allowed the nanoparticles to discretely separate on the vertical axis of the suspension depending on their weight. After slowly spreading the sample on the grids, tiny volumes from the lower part of the suspension probably managed to remain separated from the upper part. It is also worth noting that after several days, a small amount of nanoparticles settled. Consequently, we analyzed the sediment as well (Figure 7e) and observed nanoparticles with bigger sizes (around 100 nm).

**Magnetic measurements.** The specific saturation magnetization (Figure 8) of the MNP (55.6 emu/g) was higher than that of MNP@Ag (48.7 emu/g). The saturation magnetization values were calculated by extrapolating the tangent to the plot of  $M$  versus  $1/H$  at high fields, in the region where the dependence between  $M$  and  $1/H$  is a straight line. The difference in saturation magnetizations represents an indirect proof of the presence of a non-magnetic silver shell on the MNPs. Furthermore, there were small differences in both coercive fields ( $H_c$ ) and ratios between the residual and saturation magnetizations (squareness value,  $M_r/M_s$ ) of the samples (Figure 8). The MNP@Ag sample showed lower values for  $H_c$  and  $M_r/M_s$  ratios, being even closer to a superparamagnetic behavior. The superparamagnetic behavior allowed a ferrofluid-like behavior of the MNP@Ag suspension (Figure 8a) after concentration by ultracentrifugation and ultra-sonication.

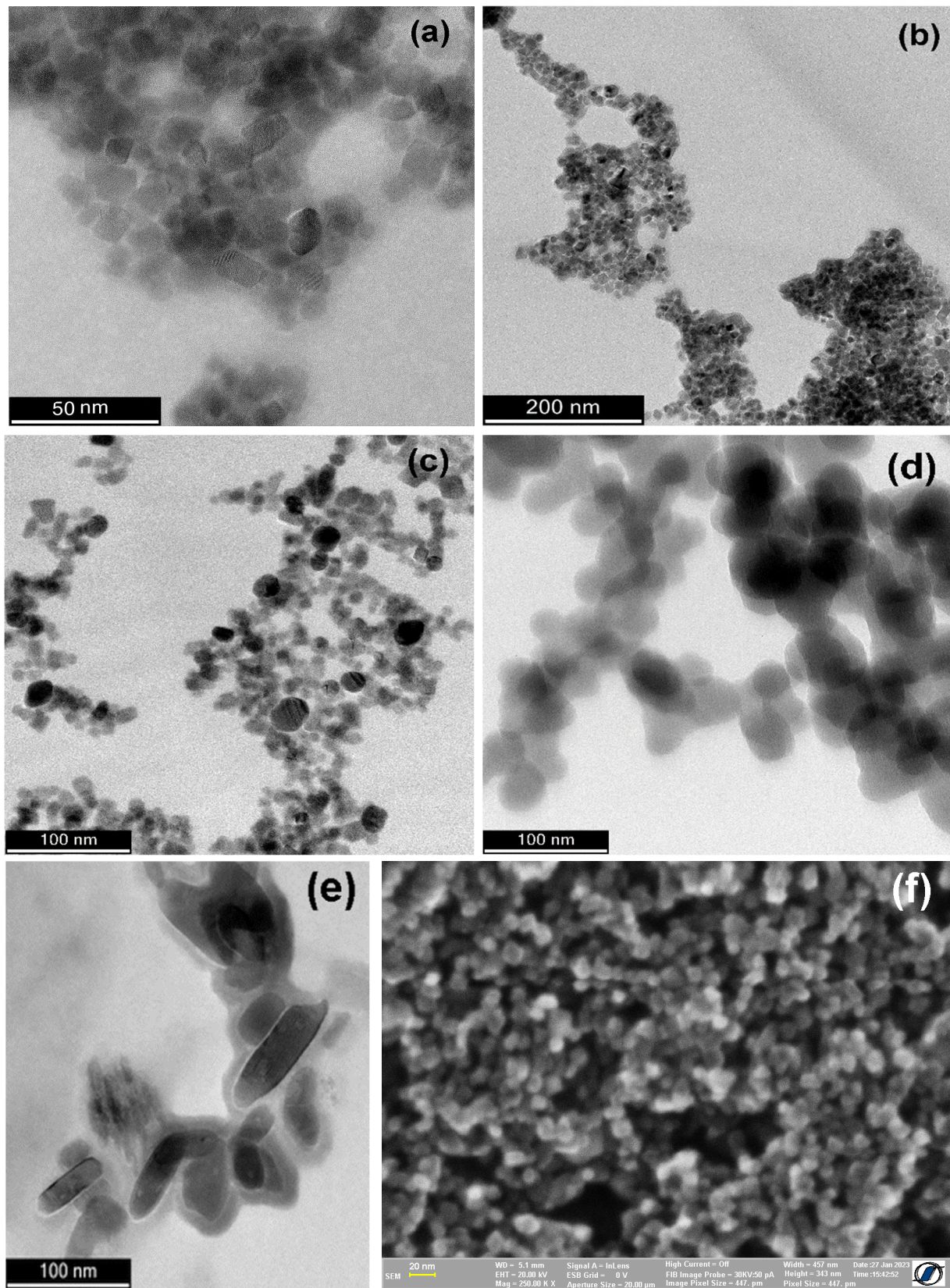


**Figure 7.** TEM images of magnetite nanoparticles (a,b) and silver-coated magnetite (c–e); SEM image silver-coated magnetite (f).

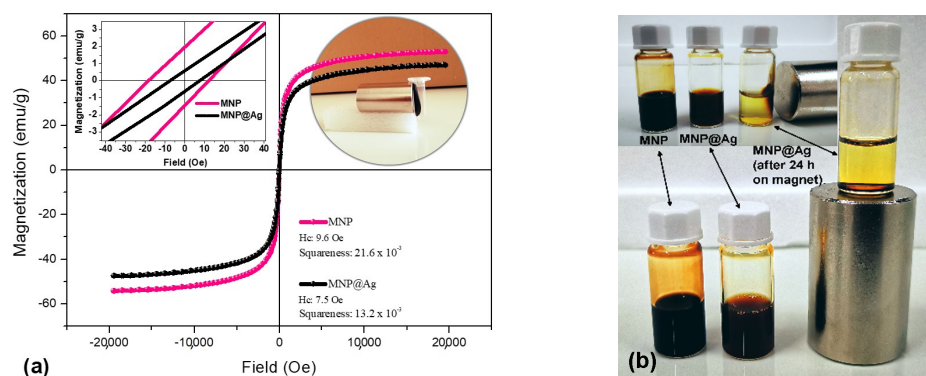


**Figure 8.** (a) Magnetization loops of the magnetic samples. Inset: details from the loops near zero magnetic field (top left) and ferrofluid-like behavior of concentrated MNP@Ag near strong NdFeB magnet; (b) images of the samples; the MNP@Ag sample was submitted to magnetic separation in its non-concentrated (i.e., as-prepared) condition.

The difference between specific saturation magnetizations of MNP and MNP@Ag was 12.4%. This means that a fraction of about 12.4% of the nanoparticles was formed by the non-magnetic silver. Since the theoretical percentage of the silver in the MNP@Ag nanoparticles was 17.9%, we can assume that the difference could be explained by a more abundant presence of the silver in the settled fraction, the latter not being taken into account by VSM measurement.

Evaluation of magnetic hyperthermia potential of MNP@Ag nanoparticles. The heating potential was investigated through an alternating magnetic field generator (HFG3 IGBT—Eldec, Germany) and an optical thermometer (Optocon, Germany). More details about the experimental setup can be found elsewhere [30]. Figure 9 shows the heating curve of the MNP@Ag nanoparticles. The alternating magnetic field (169 kA/m) was applied for 10 min until the temperature reached about 45 °C. The specific absorption rate (SAR) of the MNP@Ag nanoparticles (5 mg/mL) was 20.6 W/g. SAR is used to quantitatively measure the heating efficiency of a magnetic material and represents the mass-normalized rate of energy absorption by a (biological) object. Therefore, MNP@Ag nanoparticles showed good potential for magnetic hyperthermia applications.

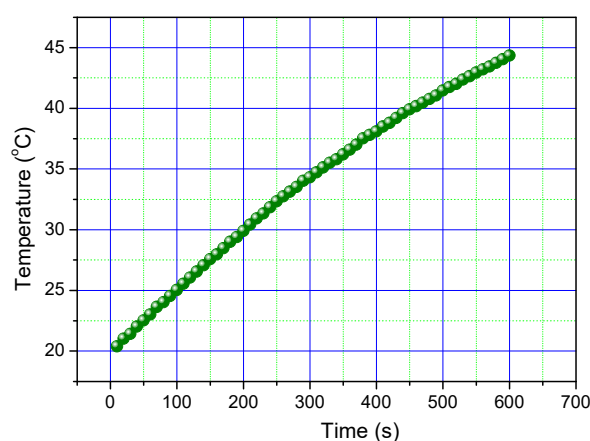


**Figure 9.** Time-dependent temperature of the heated MNP@Ag nanoparticles.

### Cell Viability

Cell viability was assessed using MTT assay at 24 h after applying, separately or in combination, the respective trigger, i.e., MNP@Ag, magnetic field (MF), hyperthermia (HT), magneto-mechanic actuation (MMA), or mitoxantrone (MTX) on cell culture.

The first tests evaluated the influence of the MNP@Ag nanoparticles on cell viability. As Figure 10 shows, a progressive decrease in viability, inversely proportional to the

nanoparticle concentration, was observed. However, the cell viability was preserved at high levels (higher than 95%) even for the highest concentration of the nanoparticles (300 µg/mL) for both types of cells. The statistical analysis (one-way ANOVA with Tukey’s post hoc test) pointed out a statistically significant difference between the viabilities of the fibroblasts and the HeLa cells, indicating a better viability for the latter.

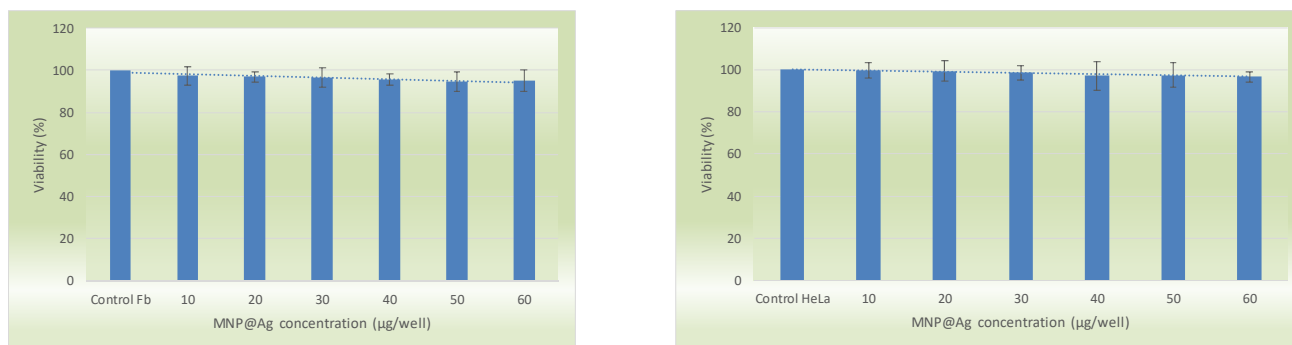


**Figure 10.** Cell viability of fibroblasts (left), and HeLa cells (right) after 24 h of incubation with MNP@Ag. Each well contained 0.2 mL cell culture medium. The difference between the two types of cells was statistically significant at the 0.05 level ( $p < 0.05$ ).

For the following tests, the highest concentration of MNP@Ag, i.e., 0.3 mg/mL, was used. As shown in Figure 11, the magneto-mechanical actuation (MMA) of MNP@Ag remained almost without effect on cell viabilities when acting alone, compared to all other interventions, administered alone or in combination, which significantly decreased the viability of both cell types.

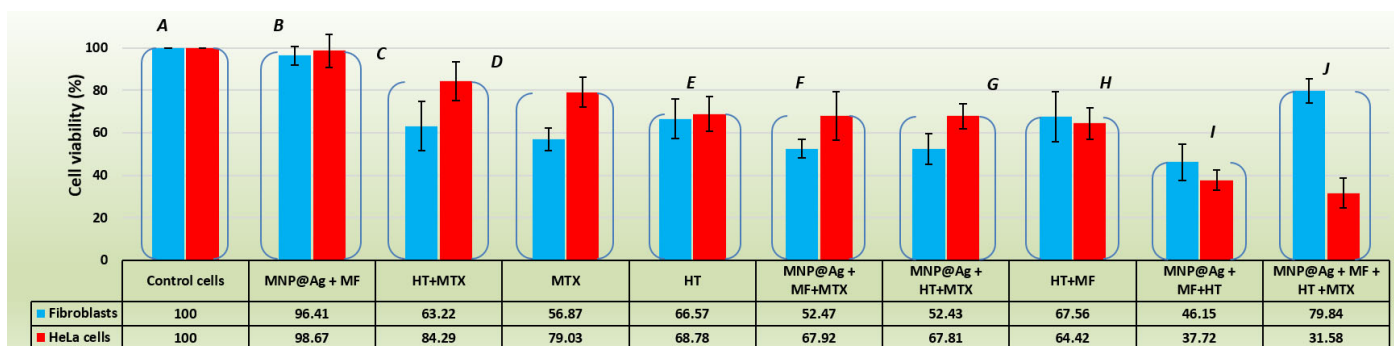


**Figure 11.** Cell viability of fibroblasts and HeLa cells after interventions with different trigger agents, i.e., magneto-mechanical actuation of MNP@Ag, hyperthermia, anti-tumor drug, and their combinations. MF stands for magnetic field while A–J letters represent the order number of each experiment.

It is interesting to note that HT alone was more effective in decreasing HeLa cell viability compared to both MTX and the combination of HT and MTX. The effect of HT was comparable to that generated by HT combined with MF, while fibroblast viability was over 60%. Furthermore, there was no difference between the magneto-mechanical actuation of nanoparticles combined with MTX (MNP@Ag + MF + MTX) on the one hand, and MNP@Ag combined with HT and MTX (MNP@Ag + HT + MTX) on the other hand.

The only intervention that appeared to be safe for fibroblasts, but highly cytotoxic for HeLa cells, was the combination of all the therapeutic triggers (MNP@Ag + MF + HT + MTX). The cytotoxic effect was not a sum of the separate effects of each involved trigger, but the result of a non-linear conjugation of the triggers in a dynamic regime imposed by the magneto-mechanical actuation of the nanoparticles.

When all the interventions (B–J) were analyzed, it could be observed that starting with H, there was a reversal in the decrease in cell viabilities. Thus, while as far as intervention

G, fibroblasts were more affected than HeLa cells, with a statistically significant difference between data sets ( $p$ , two-tailed,  $< 0.05$ ), from H to J, it was the HeLa cells that started to suffer more. The key element common to the H, I, J interventions that induced this inversion was the combination of HT and magnetic field (MF). Furthermore, when the MMA of MNP@Ag (I) was included, the effect became more significant. Finally, when MTX (J) was added, the effect on HeLa cells was greatest, with a decrease in HeLa viability up to about 32%. Moreover, this last intervention came with an interesting result, namely the reduced decrease in fibroblast viability (only 80% decrease), with a statistically significant difference compared to control cells (chi test,  $p < 0.001$ , at  $p < 0, 05$ ).

The last experiment, (J), was repeated with cells also in triplicate. The result was similar, with viabilities of about 24% for HeLa cells and about 85% for fibroblasts. This result shows that, compared to the intervention D, when only MTX was used, there was a significant improvement in therapeutic treatment against HeLa cells, suggesting a reduced need for MTX when combined with HT and MMA of MNP@Ag.

A possible explanation for this result would rely on a better permeation of the HeLa cell membrane to both MNP@Ag nanoparticles and mitoxantrone, induced by hyperthermia. Intracellular absorption of drugs has been reported to be enhanced by hyperthermia by increasing cell membrane permeability [33]. Thus, Berrios et al. [34] measured the cell membrane fluidity through direct and indirect methods, providing compelling evidence that both hot-water hyperthermia (HWH) and magnetic hyperthermia (MH) can increase membrane permeability, with the latter method inducing significantly greater effects as compared with HWH [33]. Therefore, the oscillations of MNP@Ag nanoparticles, while not affecting the cell viability by themselves, can induce a higher mobility of the antitumor drug molecules, which consequently can enter the tumor cells in a larger amount. Furthermore, due to the increased permeability induced by hyperthermia [33], the amount of drug transferred into the tumor cells is further enhanced. Therefore, cell death is mainly caused by the antitumor drug whose concentration in tumor cells was increased by MNP@Ag oscillations and hyperthermia-induced membrane permeation.

In our case, hyperthermia conditions seem to help MNP@Ag to affect cellular functions to a greater extent in the case of HeLa cells. In addition, once inside the cells, the MNPs could provide better and faster distribution of the antitumor drug.

However, the obtained results must be verified over periods longer than three days of treatment, until the total destruction of the tumor cells, also evaluating the longer-term damage to the fibroblasts.

#### 4. Conclusions

To our knowledge, this is the first report focused on the combinatorial effect of multifactorial triggers (silver-coated magnetic nanoparticles, non-magnetic hyperthermia, magneto-mechanical actuation and antitumor drug (mitoxantrone) in significantly reducing short-term tumor cell viability in vitro compared to slight, non-significant reduction of normal fibroblast cells in similar conditions. Of the nine interventions in tumor and normal cells, respectively, only one combination of the four triggers led to a strong antitumor effect while maintaining the normal cells in a safe condition in the short-term. The results need to be further investigated in terms of long-term viability and the metabolic pathways potentially involved in different cell viabilities in order to determine the possible relevance for setting up a combinatorial approach in treating malignancies.

**Author Contributions:** Conceptualization, D.D.H.; methodology, D.D.H. and C.-M.Z.-D.; formal analysis, D.D.H. and C.-M.Z.-D.; investigation, C.-M.Z.-D., G.B., A.-E.M., C.S., G.A., G.S., M.G., M.L., O.-G.D.-P. and M.T.; writing—original draft preparation, D.D.H., L.L. and C.-M.Z.-D.; writing—review and editing, D.D.H., L.L., C.-M.Z.-D. and A.-E.M.; visualization, D.D.H., L.L., C.-M.Z.-D., H.C. and N.L.; supervision, D.D.H.; project administration, D.D.H. and C.-M.Z.-D.; funding acquisition, D.D.H., L.L. and H.C. All authors have read and agreed to the published version of the manuscript.

**Funding:** This work was supported by a grant of the Ministry of Research, Innovation and Digitization CNCS–UEFIS–CDI, project number PN-III-P4-PCE-2021-1081 within PNCDI III (Contract no. 75/2022). Financial support by Romanian Ministry of Research, Innovation and Digitization, CNCS/CCCDI-UEFISCDI, Contract no. PCE20/2021 (PN-III-P4-ID-PCE-2020-2381) is also acknowledged. Financial support by Romanian Ministry of Research, Innovation and Digitization, CNCS/CCCDI-UEFISCDI, project number ERANET-EURONANOMED-3-OASIs, within PNCDI III is also acknowledged.

**Institutional Review Board Statement:** Not applicable.

**Informed Consent Statement:** Not applicable.

**Data Availability Statement:** Not applicable.

**Conflicts of Interest:** The authors declare no conflict of interest.

## References

1. Soares, S.; Sousa, J.; Pais, A.; Vitorino, C. Nanomedicine: Principles, properties, and regulatory issues. *Front. Chem.* **2018**, *6*, 360.
2. Blanco, E.; Hsiao, A.; Mann, A.P.; Landry, M.G.; Meric-Bernstam, F.; Ferrari, M. Nanomedicine in cancer therapy: Innovative trends and prospects. *Cancer Sci.* **2011**, *102*, 1247–1252.
3. Santucci, C.; Carioli, G.; Bertuccio, P.; Malvezzi, M.; Pastorino, U.; Boffetta, P.; Negri, E.; Bosetti, C.; La Vecchia, C. Progress in cancer mortality, incidence, and survival: A global overview. *Eur. J. Cancer Prev.* **2020**, *29*, 367–381.
4. Sung, H.; Ferlay, J.; Siegel, R.L.; Laversanne, M.; Soerjomataram, I.; Jemal, A.; Bray, F. Global cancer statistics 2020: GLOBOCAN estimates of incidence and mortality worldwide for 36 cancers in 185 countries. *CA Cancer J. Clin.* **2021**, *71*, 209–249.
5. Sambhi, M.; Haq, S.; Samuel, V.; Qorri, B.; Haxho, F.; Hill, K.; Harless, W.; Szewczuk, M.R. Alternative therapies for metastatic breast cancer: Multimodal approach targeting tumor cell heterogeneity. *Breast Cancer* **2017**, *9*, 85–93.
6. Moore, J.A.; Chow, J.C.L. Recent progress and applications of gold nanotechnology in medical biophysics using artificial intelligence and mathematical modeling. *Nano Express* **2021**, *2*, 022001.
7. Zhang, H.; Liu, X.L.; Zhang, Y.F.; Gao, F.; Li, G.L.; He, Y.; Peng, M.L.; Fan, H.M. Magnetic nanoparticles based cancer therapy: Current status and applications. *Sci. China Life Sci.* **2018**, *61*, 400–414.
8. Siddique, S.; Chow, J.C.L. Recent advances in functionalized nanoparticles in cancer theranostics. *Nanomaterials* **2022**, *12*, 2826. [[CrossRef](#)]
9. Flores-Rojas, G.G.; López-Saucedo, F.; Vera-Graziano, R.; Mendizabal, E.; Bucio, E. Magnetic nanoparticles for medical applications: Updated review. *Macromol* **2022**, *2*, 374–390.
10. Saji, U.; Sang, J.L.; Kondareddy, C.; Chong-Su, C.; In-Kyu, P. Polysaccharide-coated magnetic nanoparticles for imaging and gene therapy. *BioMed Res. Int.* **2015**, *2015*, 959175.
11. El-Gendy, A.A. Core/Shell magnetic nanoparticles for biomedical applications. In *Micro and Nano Technologies, Magnetic Nanostructured Materials*; El-Gendy, A.A., Barandiaran, J.M., Hadimani, R.L., Eds.; Elsevier: Amsterdam, The Netherlands, 2018; pp. 41–58. [[CrossRef](#)]
12. Shin, T.H.; Manavalan, B.; Lee, D.Y.; Basith, S.; Seo, C.; Paik, M.J.; Kim, S.W.; Seo, H.; Lee, J.Y.; Kim, J.Y.; et al. Silica-coated magnetic-nanoparticle-induced cytotoxicity is reduced in microglia by glutathione and citrate identified using integrated omics. *Part. Fibre Toxicol.* **2018**, *18*, 42.
13. León Félix, L.; Sanz, B.; Sebastián, V.; Torres, T.E.; Sousa, M.H.; Coaquira, J.A.H.; Ibarra, M.R.; Goya, G.F. Gold-decorated magnetic nanoparticles design for hyperthermia applications and as a potential platform for their surface-functionalization. *Sci. Rep.* **2019**, *9*, 4185.
14. Haribabu, V.; Girigoswami, K.; Girigoswami, A. Magneto-silver core-shell nanohybrids for theragnosis. *Nano-Struct. Nano-Objects* **2021**, *25*, 100636.
15. Rashidi Huyeh, M.; Balouchzehi, S.; Shafiee Afarani, M.; Khajegi, P. Magnetite-Silver core-shell nanoparticles: Synthesis, characterizes, and optical properties. *Plasmonics* **2022**, *17*, 2385–2390.
16. Sharaf, E.M.; Hassan, A.; AL-Salmi, F.A.; Albalwe, F.M.; Albalawi, H.M.R.; Darwish, D.B.; Fayad, E. Synergistic antibacterial activity of compact silver/magnetite core-shell nanoparticles core shell against Gram-negative foodborne pathogens. *Front. Microbiol.* **2022**, *13*, 929491.
17. Ramirez-Acosta, C.M.; Cifuentes, J.; Cruz, J.C.; Reyes, L.H. Patchy Core/Shell, Magnetite/Silver nanoparticles via green and facile synthesis: Routes to assure biocompatibility. *Nanomaterials* **2020**, *10*, 1857.
18. Park, S.B.; White, S.B.; Steadman, C.S.; Pechan, T.; Pechanova, O.; Clemente, H.J.; Thirumalai, R.V.; Willard, S.T.; Ryan, P.L.; Feugang, J.M. Silver-coated magnetic nanocomposites induce growth inhibition and protein changes in foodborne bacteria. *Sci. Rep.* **2019**, *9*, 17499.
19. Anderson, S.D.; Gwenin, V.V.; Gwenin, C.D. Magnetic functionalized nanoparticles for biomedical, drug delivery and imaging applications. *Nanoscale Res. Lett.* **2019**, *14*, 188.
20. Zhang, X.F.; Liu, Z.G.; Shen, W.; Gurunathan, S. Silver nanoparticles: Synthesis, characterization, properties, applications, and therapeutic approaches. *Int. J. Mol. Sci.* **2016**, *17*, 1534.

21. Sofi, M.A.; Sunitha, S.; Sofi, M.A.; Pasha, S.K.; Choi, D. An overview of antimicrobial and anticancer potential of silver nanoparticles. *J. King Saud Univ. Sci.* **2022**, *34*, 101791.
22. Liu, X.; Chen, J.L.; Yang, W.Y.; Qian, Y.C.; Pan, J.Y.; Zhu, C.N.; Liu, L.; Ou, W.B.; Zhao, H.X.; Zhang, D.P. Biosynthesis of silver nanoparticles with antimicrobial and anticancer properties using two novel yeasts. *Sci. Rep.* **2021**, *11*, 15795.
23. Haque, S.; Norbert, C.C.; Acharyya, R.; Mukherjee, S.; Kathirvel, M.; Patra, C.R. Biosynthesized silver nanoparticles for cancer therapy and in vivo bioimaging. *Cancers* **2021**, *13*, 6114.
24. Lopez, S.; Hallali, N.; Lalatonne, Y.; Hillion, A.; Antunes, J.C.; Serhan, N.; Clerc, P.; Fourmy, D.; Motte, L.; Carrey, J.; et al. Magneto-mechanical destruction of cancer-associated fibroblasts using ultra-small iron oxide nanoparticles and low frequency rotating magnetic fields. *Nanoscale Adv.* **2022**, *4*, 421–436.
25. Wong, S.H.D.; Xu, X.; Chen, X.; Xin, Y.; Xu, L.; Lai, C.H.N.; Oh, J.; Wong, W.K.R.; Wang, X.; Han, S.; et al. Manipulation of the nanoscale presentation of integrin ligand produces cancer cells with enhanced stemness and robust tumorigenicity. *Nano Lett.* **2021**, *21*, 3225–3236.
26. Chiriac, H.; Radu, E.; Tibu, M.; Stoian, G.; Ababei, G.; Lăbușcă, L.; Herea, D.D.; Lupu, N. Fe-Cr-Nb-B ferromagnetic particles with shape anisotropy for cancer cell destruction by magneto-mechanical actuation. *Sci. Rep.* **2018**, *8*, 11538.
27. Herea, D.D.; Labusca, L.; Radu, E.; Chiriac, H.; Grigoras, M.; Panzaru, O.D.; Lupu, N. Human adipose-derived stem cells loaded with drug-coated magnetic nanoparticles for in-vitro tumor cells targeting. *Mater. Sci. Eng. C* **2019**, *94*, 666–676.
28. Chiriac, H.; Lupu, N.; Lostun, M.; Ababei, G.; Grigoras, M.; Dănceanu, C. Low TC Fe-Cr-Nb-B glassy submicron powders for hyperthermia applications. *J. Appl. Phys.* **2014**, *115*, 17B520.
29. Herea, D.D.; Dănceanu, C.; Radu, E.; Labusca, L.; Lupu, N.; Chiriac, H. Comparative effects of magnetic and water-based hyperthermia treatments on human osteosarcoma cells. *Int. J. Nanomed.* **2018**, *13*, 5743–5751.
30. Herea, D.D.; Chiriac, H.; Lupu, N.; Grigoras, M.; Stoian, G.; Stoica, B.A.; Petreus, T. Study on iron oxide nanoparticles coated with glucose-derived polymers for biomedical applications. *Appl. Surf. Sci.* **2015**, *352*, 117–125. [[CrossRef](#)]
31. Ashraf, J.M.; Ansari, M.A.; Khan, H.M.; Alzohairy, M.A.; Choi, I. Green synthesis of silver nanoparticles and characterization of their inhibitory effects on AGEs formation using biophysical techniques. *Sci. Rep.* **2016**, *6*, 20414.
32. Sastry, M.; Mayya, K.S.; Bandyopadhyay, K. pH Dependent changes in the optical properties of carboxylic acid derivatized silver colloidal particles. *Colloids Surf. A* **1997**, *127*, 221–228.
33. Liu, X.; Zhang, Y.; Wang, Y.; Zhu, W.; Li, G.; Ma, X.; Zhang, Y.; Chen, S.; Tiwari, S.; Shi, K.; et al. Comprehensive understanding of magnetic hyperthermia for improving antitumor therapeutic efficacy. *Theranostics* **2020**, *10*, 3793–3815.
34. Alvarez-Berrios, M.P.; Castillo, A.; Mendez, J.; Soto, O.; Rinaldi, C.; Torres-Lugo, M. Hyperthermic potentiation of cisplatin by magnetic nanoparticle heaters is correlated with an increase in cell membrane fluidity. *Int. J. Nanomed.* **2013**, *8*, 1003–1013.

**Disclaimer/Publisher’s Note:** The statements, opinions and data contained in all publications are solely those of the individual author(s) and contributor(s) and not of MDPI and/or the editor(s). MDPI and/or the editor(s) disclaim responsibility for any injury to people or property resulting from any ideas, methods, instructions or products referred to in the content.